Preparation of a novel V2C mxene/g-C3N4 and its performance in plasma catalytic denitrification

Haoxuan Hu[1], Ran Zhao[1*], Xianwei Fan[1], Junyi Liu[1], Yahui Nie[1], and Dong Wang[1*]

[1]Hubei Key Laboratory of Advanced Textile Materials & Application, Hubei International Scientific and Technological Cooperation Base of Intelligent Textile Materials & Application, Wuhan Textile University, Wuhan 430200, China.

ABSTRACT. In this work, the g-C_3N_4/V_2C MXene composite catalyst was prepared by solvothermal method, and its denitration performance under synergistic plasma (NTP) was investigated. The results showed that when the mass ratio of V_2C is 3%, the denitration performance of V-CN-3-NTP is as high as 83.3%, which is 1.2 and 2.1 times that of the V_2C-NTP and g-C_3N_4-NTP systems alone. The apparent morphology, phase structure, and catalytic mechanism of the catalyst were studied by SEM, TEM, XRD, FTIR, XPS, etc. The results showed that g-C_3N_4 grows well on V_2C mxene. V_2C is not only an electron acceptor but also an active site for NO adsorption. The electrons and holes generated by V_2C could be effectively separated by the high-voltage electric field, which improves the denitration performance and shows a good synergistic effect.

1 INRTODUCTION

The exhaust gas emitted from human production and life has caused a lot of irreversible harm to the environment, and nitrogen oxides (NO_x), as the most difficult part of exhaust gas treatment, has seriously affected people's daily life[1]. As a new type of gas pollutant treatment technology, plasma denitration technology improves the technical defects of traditional denitration process such as high energy consumption and high cost, and avoids the reducing agent required in SCR (selective catalytic reduction), and does not produce secondary pollution[2], which is one of the most promising and effective technologies in the treatment of air pollution. During the discharge process, the breakdown gas generates high-energy electrons to provide energy for the reaction, thereby generating a series of reactive groups (such as N^* and O^*), and these reactive groups react with NO gas molecules to form harmless substances. So far, plasma denitration technology still has some drawbacks (large power consumption, relatively low denitration efficiency, etc.). Therefore, in order to solve these problems, the denitration reaction with the catalysts-NTP synergistic method has become a hot research topic.Wang[3]et al. reported a new type of 12Mn-12Cu/ZSM5 catalyst in the plasma-catalyst system. The results showed that the combination of plasma and the catalyst improved the removal efficiency of NO, and the introduction of Mn improved the performance of the Cu/ZSM5 catalyst.Yu[4] et al. divided the catalytic process of the plasma-assisted catalyst into two stages: in the first stage, NO_x were adsorbed by the catalyst (not discharged); in the second stage, using N_2 and Ar as carrier gas, the adsorbed NO_x were decomposed into N_2 And O_2. The instantaneous increase of active oxygen groups was the main reason for improving the conversion of NO_x, and solid carbon was added as a trapping agent for active oxygen groups to increase the conversion rate of NO_x in the N_2 plasma. However, in order to improve the denitration efficiency, many researchers used metals as catalysts, which were too costly and may cause metal pollution. Most of the relative studies require the addition of reducing agents (such as CH_4 and NH_3) to the reaction system, which did not exert the synergistic effect of this kind of system. This work aimed to construct a cheap new plasma synergistic catalytic system to overcome these problems.

g-C_3N_4 (graphite phase carbon nitride), as a non-metallic material, has attracted attention in the field of catalysis due to its suitable band gap ,easy synthesis, low cost, and good physical and chemical properties[5]. However, its lower carrier separation efficiency and smaller specific surface area limited its practical application in the field of catalysis. Therefore, researchers have made efforts to improve its performance defects, and through a series of methods (such as surface control[6], doping[7] and formation of heterojunctions with semiconductors[8]), the separation efficiency and specific surface area of electrons and holes have been increased, and the specific surface area has been increased. The active sites on the surface further increased the activity of the catalyst[9]. The electrons of g-C_3N_4 was migrated by the high-voltage electric field, which improved its reduction performance and facilitated the reduction of NO[10]. In this work, a one-dimensional tubular g-C3N4 is prepared, which exposed more active sites under the support of a large specific surface area, thereby improving its denitration performance.

Transition metal carbides and nitrides (called MXenes)

*Corresponding authors. E-mail address:ranzhao.hust@gmail.com(R.zhao),wangdon08@126.com(D.Wang)

are one of the latest 2D materials. Since Naguib et al[11] first developed Ti_3C_2, they have promoted a lot of research, are widely used, and show excellent performance. In addition, the large specific surface area and abundant surface functions made MXenes effective adsorbents for various molecular and ionic species, expanding their applications in ion screening, catalysts and sensors[12-14]. Vanadium carbide (V_2C) is a typical MXene material, which has similar properties to titanium carbide (Ti_3C_2), has metal conductivity and hydrophilicity, and has excellent chemical stability and light stability[15]. Among them, good thermal stability is an important prerequisite for maintaining good properties in plasma[16]. V_2C was mostly used in energy storage and conversion, such as batteries, capacitors, etc[17-19].But due to its excellent performance, it had a very broad prospect in catalysis. This article applies V_2C to the field of catalysis for the first time, and uses it with g-C_3N_4 for denitration in the plasma-catalysts system .

In this work, the solvothermal method was used to grow V_2C etched by HF on the dicyandiamide supramolecular precursor, and then calcined at high temperature to generate V_2C/CN composite. Under the action of the low-temperature plasma synergistic catalyst, the denitration performance of the V_2C/CN composite reaches up to 83.3%, which is 2.1 and 1.2 times that of the CN-NTP system and the V_2C-NTP system alone. In addition, characterization techniques were used to study the properties of the catalyst, and the synergistic mechanism of V_2C/CN and NTP was studied.

2 EXPERIMENTAL SECTION

2.1 Synthesis of V_2C

In an ice bath, V_2AlC (1 g) powder was slowly added to 20 mL of hydrofluoric acid (48%) within 5 minutes and stirred the above mixture vigorously at 35°C for 24 hours, then increased the temperature to 50°C and continue stirring for 48 hours. The as-prepared suspension was then centrifuged, and the obtained solids were washed repeatedly with deionized water until the pH value is close to neutral (>6), and then freeze-dry to obtain V_2C MXene powder[15].

2.2 Synthesis of V_2C/g-C_3N_4

3 g of dicyandiamide (DCDA) was added to a mixed solvent consisting of deionized water and isopropanol (water/isopropanol volume ratio=1:2), and stirred for 30 min. Then a certain amount of V_2C was added to the mixed solution and stirred, and then the obtained solution was transferred to a 25mL autoclave and kept at 180°C for 10 hours. After the reaction was completed, the product was centrifuged to obtain a supramolecular precursor. Then, washed three times with water and ethanol to remove the remaining solvent, and then dried in a vacuum at 80°C overnight. Finally, the supramolecular precursor was heated to 550°C at a heating rate of 10°C/min, and stored in the air for 2 hours to generate a g-C_3N_4(CN)/V_2C sample. The final products were designated as C/V-1, C/V-2, C/V-3, and C/V-4, corresponding to the weight of V_2C MXene to dicyandiamide (1, 2, 3, and 4 wt %)[20].

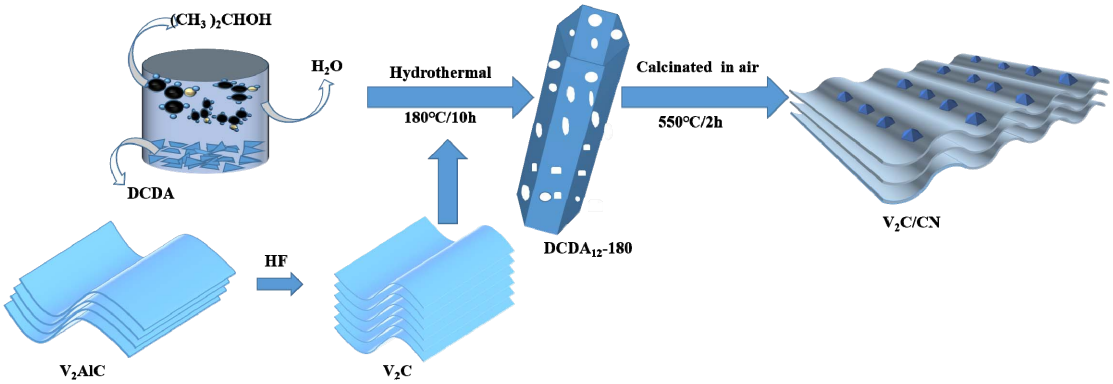

Scheme 1. Schematic Diagram of the Synthesis Process of the V_2C/g-C_3N_4 catalyst

2.3 Characterization

The crystal phase was determined by X-ray diffraction (XRD, Bruker D8 Advance, Germany, Cu Kα). The X-ray photoelectron spectra (XPS) of samples were collected by a spectrometer(Thermo Fischer , ESCALABXi+, Al-Kα). The morphologies of materials were characterized on a scanning electron microscope (SEM, JSM-IT300A), The Brunauer Emmett Teller surface area (BET) was obtained by N_2 adsorption−desorption isotherms measured at 77 K on a surface area analyzer (Micromeritics, ASAP2460), and pore structural parameters were determined by the Barrett−Joyner−Halenda (BJH) method. Thermogravimetric analysis (TGA) was carried out using a NETZSCH STA 449F3 instrument under a nitrogen atmosphere.

2.4 Experimental procedure and apparatus

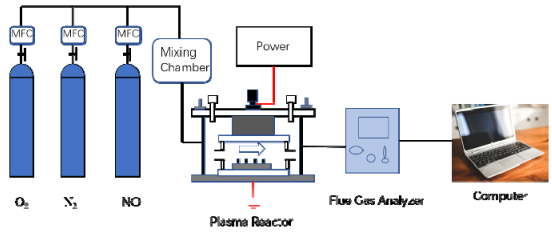

Fig. 1 Schematics of experimental apparatus.

The NO denitrification device consists of a gas generator, a dielectric barrier discharge (DBD) reactor, and a gas detection device (as shown in the Fig. 1). The simulated flue gas is composed of 500ppm NO, 8% O_2 and N_2 balance gas. Use a flow controller (MFC) to control the gas flow at 500 mL/min. The experimental sample is 0.5g. The inlet and outlet NO and NO_2 concentrations are analyzed online with KM950 flue gas analyzer. All tests are performed at atmospheric pressure and room temperature. The denitration efficiency is calculated as follows:

$$\eta = (1-C/C_0) \times 100\%$$

where η is the denitration rate (%), C_0 is the inlet NO concentration(ppm) and C is the outlet NO concentration (ppm).

The two stainless steel electrodes (φ50×15mm) are high voltage electrodes and ground electrodes. The distance between the two electrodes is 10 mm. The DBD (φ60×8mm, DBD-100B, Nanjing Suman Electronics Co., Ltd., China) reactor made of quartz glass is placed between the two electrodes.

3 RESULTS AND DISCUSSION

3.1.SEM

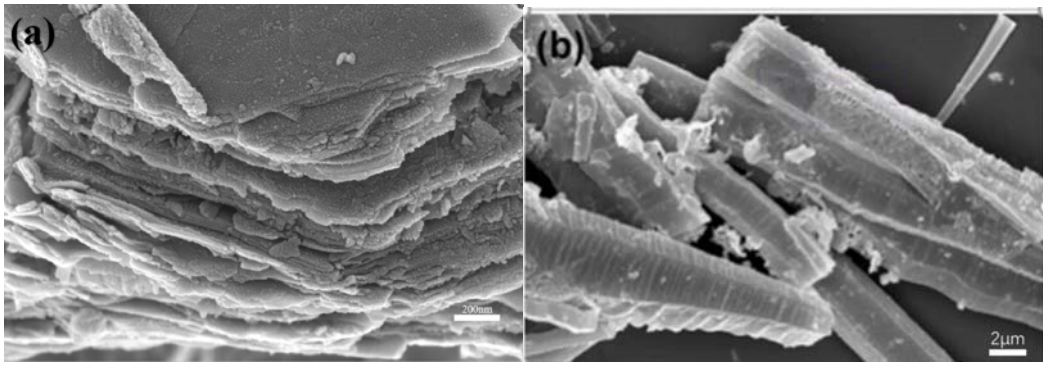

Fig. 2 SEM images of (a)V_2C;(b) g-C_3N_4

The morphology and microstructure of the prepared catalyst were analyzed by SEM. As shown in Fig. 2(a), the V_2AlC precursor was etched in HF and freeze-dried in a liquid environment to obtain a good two-dimensional layered structure, and clearly depicted very thin two-dimensional flakes. Obviously, hydrothermal treatment transformed DCDA12-180 into a 1D hexagon. It's important to note that subsequent calcination of DCDA12-180 at 550°C produced 1D mesoporous g-C_3N_4 microtubes, retaining the 1D hexagonal microtubular morphology (Fig. 2b). Volume shrinkage occurred during high-temperature calcination, which could be attributed to the formation of a denser structure with a higher degree of polymerization.

3.2 XRD

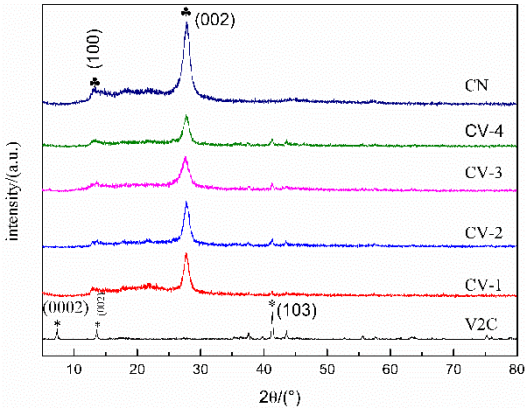

Fig. 3 XRD patterns of as-obtained catalysts

X-ray diffraction technology was used to analyze the phase and crystal structure of the catalyst. The analysis results are shown in Fig. 3, and the results confirmed the successful synthesis of CN, V_2C and V_2C/CN composite. Two main XRD peaks can be clearly found in the V_2C spectrum, corresponding to approximately 13.6° and 41.2° respectively. And after HF etching, a new XRD peak appeared at about 7.1°, corresponding to the (0002) crystal plane of V_2C, indicating the successful synthesis of V_2C[15]. There are two typical XRD peaks of graphite phase carbon nitride in the CN spectrum, at about 13.0° and 27.8°, corresponding to the in-plane tri-s-triazine motifs packing of CN and the interlayer of conjugated aromatic segments, respectively[20]. Due to the weak strength and low V_2C content, the (0002) crystal plane of V_2C is not observed in the V_2C/CN composite, but other

characteristic peaks of V_2C and CN can be clearly found on the spectrum. It shows the successful synthesis of V_2C/CN.

3.3 TG

As shown in Fig. 4, the thermogravimetric curves of V_2C, CN, and CV-3 from 25°C to 800°C in a nitrogen atmosphere were characterized. The results showed that the weight loss rate of the catalyst decreases in、

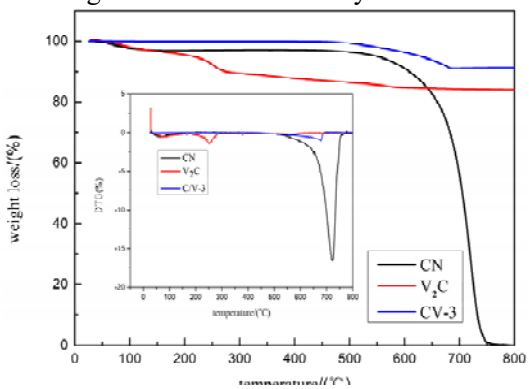

Fig. 4 TGA curves of V2C, CN, and CV-3 composite

the following sequence: CN (100%)>V2C (15.97%)>CV-3 (8.85%). It can be seen that the thermal stability of CV-3 is much higher than that of CN and V_2C. The thermal decomposition process of V_2C is divided into two stages. The first stage occurred at 280°C. Most of the decomposition is attributed to the loss of crystalline water and water adsorbed by the stream. The second stage is from about 300°C to 800°C. °C, due to the loss of OH/O/F functional groups, in this process, OH/O/F is released in the form of H_2O, O_2, HF[16]. CN was decomposed once at about 550°C to 750°C. At this time, the structure of CN was completely destroyed and CN was completely decomposed[21]. The thermal decomposition process of CV-3 can be divided into three stages, including the decomposition of oxygen-containing functional groups produced by the mutual bonding of V_2C and CN (430°C to 530°C), the decomposition of functional groups in V_2C and the collapse of CN structure (530°C to 630°C) and the decomposition of CN (630°C to 700°C). It can be concluded that the addition of V_2C greatly improves the thermal stability of CN, enabling it to maintain a relatively stable structure at high temperatures.

3.4 XPS

XPS was used to analyze the surface atomic composition and valence of C/V-3. The measured energy spectrum of C/V-3 clearly shows that the synthesized composite material contains V, N, O and C elements (Fig. 5(a)), indicating the formation of V_2C/CN phase. By analyzing the N 1s peak (Fig. 5(c)), it was determined that the binding energies of N 1s were 398.67 eV and 400.20 eV, 401.30ev, respectively. which can be attributed to C-N=C, N-$(C)_3$, C-N-H[20]. For O 1s (Fig5. (b)), the observed peak can be decomposed into four components, including C-V-OH_x(532.01 eV), C-V-O_x (532.40 eV),C=O(533.66ev) and VO_x (530.15 eV)[21]. The deconvoluted V 2p (Fig5. (d)) shows V 2p1/2 at 513.51 eV and V 2p3/2 at 521.41eV, indicating the presence of V^{2+}, which can be attributed to the remaining unreacted MAX phase in the prepared MXene and the same binding energy the overlap of the lower V−C peak. V 2p1/2 at 516.62 eV and V 2p3/2 at 524.86 eV correspond to V^{4+} and VO_2(P) of V_2C, respectively[19]. The C 1s area (Fig5. (e)) shows the existence of V−C (284.89 eV), C−C (288.47eV), C−OH (286.60 eV) and C=O (293.43 eV). XPS analysis results further prove that V_2C has been successfully compounded on the CN substrate.

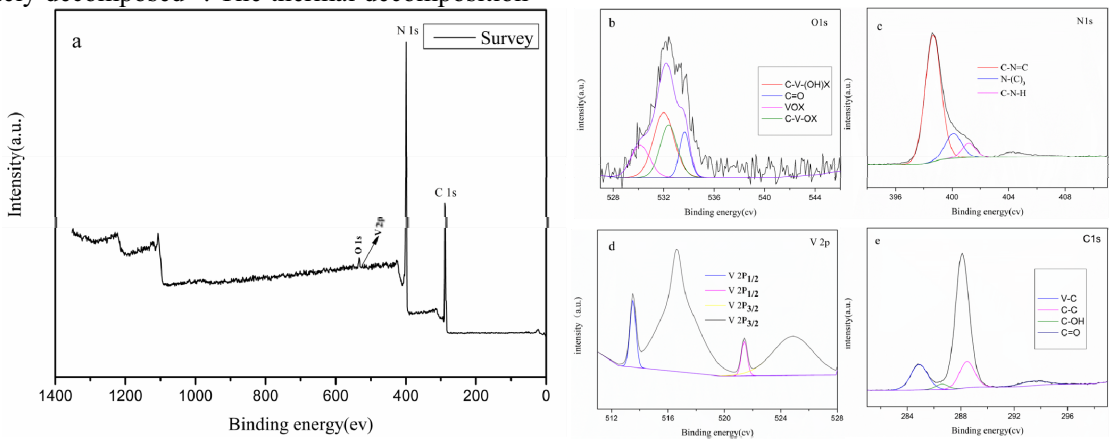

Fig. 5 (a) XPS survey spectra and high-resolution XPS spectra of (b) O1s; (c) N 1s; (d) V 2p ;(e) C1s

3.5 Denitration experiment

The denitration effect of all samples is significant, and reaches the maximum value quickly within the first 6 minutes. Then, with the reduction of NO and the formation of by-products, the by-products gradually blocked the reaction sites of the catalyst, and the denitration performance began to slowly decrease and finally reached an equilibrium value. The results show that the V_2C/CN-NTP system has better denitration performance than the single NTP system (28.1%), the

CN-NTP system (35.2%) and the V_2C-NTP system (60.6%). Among them, the V_2C/CN-NTP system showed the best denitration performance, which was 2.1 and 1.2 times that of the CN-NTP system and the V_2C-NTP system, respectively. Therefore, it also proved that there is a synergistic effect between V_2C/CN and NTP (as shown in the Fig. 6).

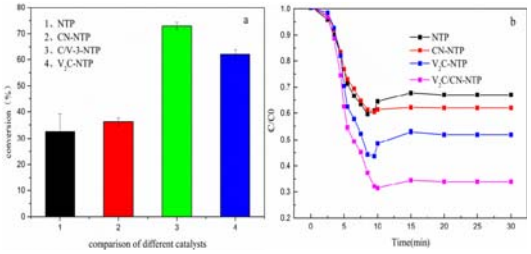

Fig. 6(a)Removal of NO with different treatment process. Conditions: simulated flue gasN2/O2/NO=72%/8%/20% (b) Comparison of V_2C、CN and CV-3 coupled NTP removal NO efficiency

3.6 BET

As shown in the Fig. 7, the specific surface area and pore structure of g-C_3N_4, V_2C and C/V-3 composite materials were studied by the N2 adsorption-desorption analysis method. Although the three samples have type IV isotherms with H3 hysteresis loops, verifying the existence of the mesoporous structure, their specific surface area and pore volume are relatively low (as shown in the table. 1). A sharp peak from 2 to 20 nm is observed in the pore size distribution curve (as shown in the figure 7(a)).This indicates that g-C_3N_4 has a relatively uniform pore distribution and mesoporous characteristics[20]. Interestingly, the specific surface area of the binary C/V-3 composite material and the pore volume is higher than that of a single CN and V_2C. This may be due to the formation of CN between the V2C layers that will expand the V2C layers and increase the BET specific surface area and pore volume. The high specific surface area can provide abundant active reaction sites. And promote more NO molecules to be adsorbed on its surface[22]. Therefore, it can be concluded that compared with a single sample, the specific surface area helps to improve the photocatalytic activity, but it is not the key to improving the photocatalytic efficiency of the system Factors. As shown in the table.1,

Table. 1 Textural Properties of V_2C, g-C_3N_4, and C/V-3

sample	S_{BET} (m^2g^{-1})	V_{total}(cm^3g^{-1})
V_2C	5.1890	0.04
g-C_3N_4	34.2663	0.087
C/V-3	44.6565	0.25

Compared with the pure CN sample, the SBET of C/V-3 increased by 39.4675$m^2g^{-1}$and V_{total} increased by 0.21cm^2/g^{-1}, which indicates that the large S_{BET} and excellent adsorption performance of the composite are due to g-C3N4. In general, the adsorption capacity of the catalyst is significantly improved. The improved NO adsorption function can promote the photocatalytic oxidation process[23].

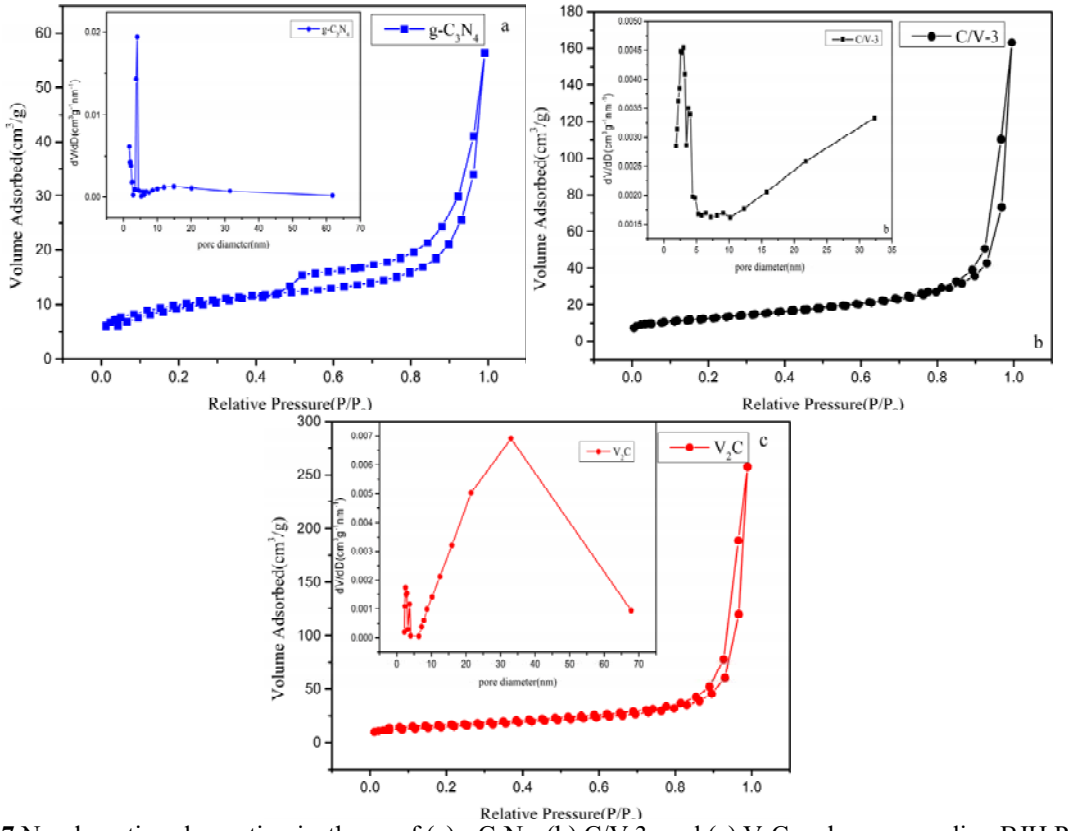

Fig. 7 N_2 adsorption-desorption isotherm of (a)g-C_3N_4; (b) C/V-3; and (c) V_2C and corresponding BJH PSD curves(inset)

4 Mechanism analysis

As shown in the fig.8, the mechanism of the V_2C/g-C_3N_4-NTP synergistic effect was studied. The high-energy electrons generated by the plasma convert N_2 into N^* and adsorbed N_2(eq 2). In addition, due to the active groups generated during the discharge process, g-C_3N_4 is excited, and the electrons in the valence band position of g-C_3N_4 are excited to conduction. The electrons in the conduction band of g-C_3N_4 are transferred to the valence band of V_2C due to the built-in electric field, and the holes are formed in the valence band, which significantly enhances the separation of electrons and holes[24]. Part of the high-energy electrons can also be injected into the conduction band of g-C_3N_4 by hitting its surface. The electrons and injected electrons participate in the conversion process of NO adsorbed on the surface of the g-C_3N_4 catalyst. Finally, NO is reduced to produce N_2 and O_2(eqs 3-5). At the same time, the O^* and O_3 produced during the reaction oxidize NO to intermediate product NO_2(eq 6), and then NO_2 reacts with N^* to be reduced to N_2 and O_2(eqs 7-11). Therefore, the high-energy electric field generated by the plasma can also effectively separate electrons and holes. In return, the g-C_3N_4 catalyst changed the discharge method and made the discharge more uniform. This synergistic effect improved the NO conversion rate and energy efficiency[10].

$$\text{V-CN-3+plasma} \rightarrow V_2C(e^-)+\text{g-}C_3N_4(h^+) \quad (1)$$

$$N_2+e^-(p) \rightarrow N+N+e^-(p) \quad (2)$$

$$NO+N \rightarrow N_2+O \quad (3)$$

$$O_2+e^-(p) \rightarrow O+O+e^-(p) \quad (4)$$

$$O_2+O \rightarrow O_3 \quad (5)$$

$$NO+O \rightarrow NO_2 \quad (6)$$

$$NO+O_3 \rightarrow NO_2+O_2 \quad (7)$$

$$N_2+e^- \rightarrow e^-+N_2(A) \quad (8)$$

$$N_2(A)+NO \rightarrow N_2+N+O \quad (9)$$

$$N_2(A)+N_2O \rightarrow 2N_2+O \quad (10)$$

$$NO_2+N \rightarrow N_2+O_2 \quad (11)$$

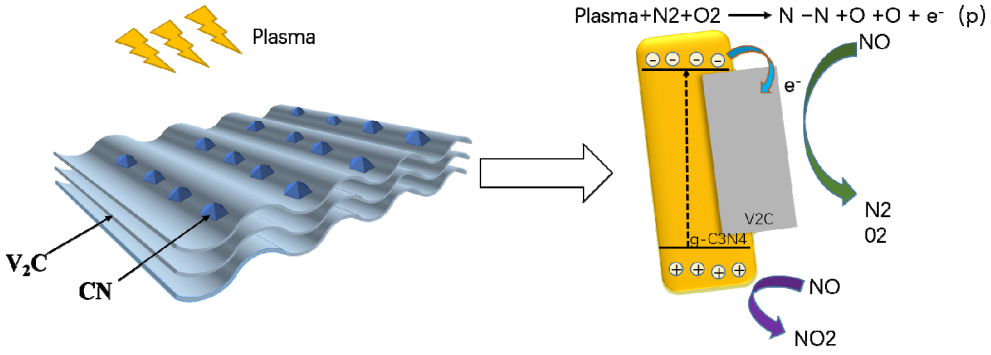

Fig. 8 Reaction mechanism

5 Conclusions

In this work, a new g-C3N4/V2C MXene catalyst has been successfully synthesized, and used for plasma denitration technology for the first time. The optimized composite C/V-3 showed an improved NO removal of 83.3% in the high-energy electric field, which is 1.2 and 2.1 times higher than V_2C-NTP and g-C_3N_4-NTP systems alone, respectively. The electrons transferred to V2C and the injected electrons react with the generated active

groups to reduce NO to N2 and O2. G-C_3N_4 can be excited by high-energy electric field and then can transfer electrons to V_2C MXene which facilitates the separation of electron−hole pairs. The synergistic effects of catalysts-plasma system promoted the transfer of electrons. The results of this study reveal the significant potential of V_2C MXene for application in the denitration technology field.

References

1. Fan, W.; Chan, K. Y.; Zhang, C.; Zhang, K.; Ning, Z.; Leung, M. K. H., A feasibility study **225**, 535-541(2018).
2. Li, X.; Zhang, C.; Zhang, X.; Li, W.; Tan, P.; Ma, L.; Fang, Q.; Chen, G., Chemical Engineering Journal **335**, 483-490(2018).
3. Wang, T.; Zhang, X.; Liu, J.; Liu, H.; Wang, Y.; Sun, B., Applied Thermal Engineering **130**, 1224-1232(2018).
4. Yu, Q.; Wang, H.; Liu, T.; Xiao, L.; Jiang, X.; Zheng, X., Environmental science & technology **46**, 2337-44(2012).
5. Majdoub, M.; Anfar, Z.; Amedlous, A., ACS Nano **14** (10), 12390-12469(2020).
6. Liao, J.; Cui, W.; Li, J.; Sheng, J.; Wang, H.; Dong, X. a.; Chen, P.; Jiang, G.; Wang, Z.; Dong, F., Chemical Engineering Journal **379**, 122282(2020).
7. Wu, S.; Yu, H.; Chen, S.; Quan, X., ACS Catalysis **10** (24), 14380-14389(2020).
8. Xing, Y.; Yin, L.; Zhao, Y.; Du, Z.; Tan, H.-Q.; Qin, X.; Ho, W.; Qiu, T.; Li, Y.-G., ACS Applied Materials & Interfaces **12** (46), 51555-51562(2020).
9. Lu, N.; Bao, X.; Jiang, N.; Shang, K.; Li, J.; Wu, Y., Topics in Catalysis **60** (12), 855-868(2017).
10. Lu, N.; Sun, D.; Zhang, C.; Jiang, N.; Shang, K.; Bao, X.; Li, J.; Wu, Y., Journal of Physics D: Applied Physics **51** (9), 094001(2018).
11. Naguib, M.; Kurtoglu, M.; Presser, V.; Lu, J.; Niu, J.; Heon, M.; Hultman, L.; Gogotsi, Y.; Barsoum, M. W., **23** (37), 4248-4253(2011).
12. Zhu, J.; Ha, E.; Zhao, G.; Zhou, Y.; Huang, D.; Yue, G.; Hu, L.; Sun, N.; Wang, Y.; Lee, L. Y. S.; Xu, C.; Wong, K.-Y.; Astruc, D.; Zhao, P., Coordination Chemistry Reviews **352**, 306-327(2017).
13. Zhang, Y.; Wang, L.; Zhang, N.; Zhou, Z., RSC Advances **8** (36), 19895-19905(2018).
14. Sinha, A.; Dhanjai; Zhao, H.; Huang, Y.; Lu, X.; Chen, J.; Jain, R., TrAC Trends in Analytical Chemistry **105**, 424-435(2018).
15. Huang, D.; Xie, Y.; Lu, D.; Wang, Z.; Wang, J.; Yu, H.; Zhang, H., **31** (24), 1901117(2019).
16. Wu, M.; Wang, B.; Hu, Q.; Wang, L.; Zhou, A., **11** (11), 2112(2018).
17. Wu, X.; Wang, H.; Zhao, Z.; Huang, B., Journal of Materials Chemistry A **8** (25), 12705-12715(2020).
18. Liu, F.; Liu, Y.; Zhao, X.; Liu, K.; Yin, H.; Fan, L. Z., Small **16** (8), e1906076(2020).
19. Wang, Z.; Yu, K.; Feng, Y.; Qi, R.; Ren, J.; Zhu, Z., ACS Applied Materials & Interfaces **11** (47), 44282-44292(2019).
20. Liu, Q.; Chen, C.; Yuan, K.; Sewell, C. D.; Zhang, Z.; Fang, X.; Lin, Z., Nano Energy **77**, 105104(2020).
21. Yao, C.; Wang, R.; Wang, Z.; Lei, H.; Dong, X.; He, C., Journal of Materials Chemistry A **7** (48), 27547-27559(2019).
22. Di, J.; Xia, J.; Ji, M.; Wang, B.; Yin, S.; Zhang, Q.; Chen, Z.; Li, H., Applied Catalysis B: Environmental **183**, 254-262(2016).
23. Wang, H.; Zhao, R.; Qin, J.; Hu, H.; Fan, X.; Cao, X.; Wang, D., ACS Applied Materials & Interfaces **11** (47), 44249-44262(2019).
24. Tang, Q.; Sun, Z.; Deng, S.; Wang, H.; Wu, Z., Journal of Colloid and Interface Science **564**, 406-417(2020).